



# INFLUENCE OF HOMOGENIZATION PRECEDING TO COLD-ROLLING ON THE MICROSTRUCTURE OF THE AA-3003

## INFLUENCIA DEL HOMOGENEIZADO PREVIO AL LAMINADO EN FRÍO EN LA MICROESTRUCTURA DEL AA3003

Gennifer Aparicio-Carrillo<sup>1</sup> , Marco Ciaccia-Sortino<sup>2,\*</sup> , Ricardo Jerez G<sup>3</sup>

Received: 09-06-2020, Received after review: 09-04-2021, Accepted: 11-05-2021, Published: 01-07-2021

### Abstract

The aluminum alloy AA3003 produced by a direct chill continuous casting process has a microstructure that significantly affects its potential use in engineering applications. This work studies the effects of the homogenizing heat treatment on the microstructure of AA3003 with cold working. Six conditions were studied, combining the variables initial condition (with and without homogenizing) and amount of cold working. All conditions were evaluated by means of optical and scanning electron microscopy, in combination with backscattered electrons and energy dispersive X ray spectroscopy techniques. Results suggest that for both initial conditions, the secondary phases present are  $Al_6(Mn,Fe)$  and  $\alpha-Al(Mn,Fe)Si$ , which vary in number, size, and shape. The homogenization caused the dissolution and precipitation of dispersoids, in addition to the spheroidization of primary particles, and minor variation of the size of secondary particles during cold working. Secondary phases are composed of primary and secondary particles, which differ in their Fe and Mn content, resulting in a lower Mn/Fe ratio for the primary particles (0,57 for the as-received condition and 0,80 for the homogenized condition), whereas the dispersoids have a higher Mn/Fe ratio (1,56 after the homogenization). Homogenization increased ductility and reduced the likelihood of cracking during cold working. This was evidenced by the results obtained for strength, hardness, and ductility.

**Keywords:** Microstructure, AA-3003, homogenized, cold work, continuous casting

### Resumen

La aleación de aluminio AA3003 proveniente de colada continua posee una microestructura que afecta significativamente su uso potencial en aplicaciones de ingeniería. Este trabajo estudia los efectos de la homogeneización sobre la microestructura del AA3003 con trabajo en frío. Se estudiaron seis condiciones combinando las variables: condición inicial (con y sin homogeneizado) y cantidad de trabajo en frío. Se evaluaron todas las condiciones mediante microscopía óptica y electrónica de barrido, combinadas con técnicas de electrones retrodispersados y espectroscopía de dispersión de rayos X. Los resultados sugieren que, para ambas condiciones iniciales, las fases secundarias presentes son  $Al_6(Mn,Fe)$  y  $\alpha-Al(Mn,Fe)Si$ . La homogeneización causó la disolución y precipitación de los dispersoides, la esferoidización de las partículas primarias y permitió que la variación del tamaño de las partículas secundarias fuese mínima durante el trabajo en frío. Además, se obtuvo que las fases secundarias están compuestas de partículas primarias y secundarias, que difieren en su contenido de Fe y Mn, lo que resulta en una relación Mn/Fe más baja para las partículas primarias (0,57 para la condición recibida y 0,80 para la condición homogeneizada), mientras que los dispersoides tienen una mayor relación Mn/Fe (1,56 después de la homogeneización). La homogeneización aumentó la ductilidad y redujo la probabilidad de agrietamiento del material durante el trabajo en frío, lo cual se evidenció en los resultados obtenidos de resistencia, dureza y ductilidad.

**Palabras clave:** microestructura, AA3003, homogeneizado, trabajo en frío, colada continua

<sup>1,\*</sup>Centro de Investigaciones en Mecánica, Universidad de Carabobo -Venezuela.

<sup>2</sup>Ingeniería Mecatrónica, Universidad Técnica del Norte, Ecuador  
Corresponding author ✉: mciaccia@utn.edu.ec.

<sup>3</sup>Universidad de Carabobo, Escuela de Ingeniería Mecánica, Venezuela.

Suggested citation: Aparicio-Carrillo, G.; Ciaccia-Sortino, M. and Jerez G., R. (2021). «Influence of homogenization preceding to cold-rolling on the microstructure of the AA-3003». INGENIUS. N.º 26, (july-december). pp. 99-110. DOI: <https://doi.org/10.17163/ings.n26.2021.09>.

## 1. Introduction

The AA-3003 aluminum alloy is widely used in the industries of transportation vehicles body manufacturing, and food and beverage packaging, among other applications, and is commonly produced by continuous or semi continuous casting processes.

In the direct chill (DC) continuous casting process, a feed channel brings the molten metal to a rolling mill by a feed channel, at the end of which is a nozzle that distributes the metal throughout the width of the rollers. A water-cooling system maintain the rollers at a lower temperature than the molten metal, causing the solidification of the material in contact with the roller, with high cooling rates.

Therefore, the aluminum matrix becomes highly saturated with manganese and shows a variation of the microstructure with respect to the thickness, since the temperature gradients produce a faster cooling on the surfaces of the sheet than in the middle of the thickness [1].

After solidification, the microstructure is characterized by a heterogeneous solution with primary particles of  $Al_6(Mn,Fe)$  and smaller amounts of  $\alpha-Al(Mn,Fe)Si$  formed at the edges of the solidification cell or in the interdendritic areas. This microstructure significantly affects the mechanical properties of the alloy and its potential use in engineering applications [2].

To reduce this effect, a homogenization heat treatment is applied at temperatures between 500 °C and 650 °C, for a minimum of 8 h [3, 4]. This process reduces the concentration of manganese and controls the size, density, and distribution of the primary and dispersoid particles, which are some of the factors that affect the phenomenon of recrystallization, the texture, and mechanical properties of the alloy in forming stages [5, 6].

This work presents a comparative study of the microstructure of the AA-3003 aluminum alloy from continuous casting with and without homogenization, and with subsequent application of cold working (CW) by rolling, using optical and scanning electron microscopy in combination with back scattered electron and energy dispersive X-ray spectroscopy techniques, and the evaluation of its mechanical properties (microhardness and strength).

The results obtained will allow the comparison of the shape and distribution of the primary and secondary (dispersoids) particles present in the alloy in both initial conditions and after the application of cold work, to evaluate the relevance, from the microstructural point of view, of the homogenization for the subsequent forming of the alloy.

## 2. Materials y methods

### 2.1. Experimentation

A sheet of AA 3003 alloy, 1350 mm wide, 250 mm long (rolling direction) and an average thickness of 6.2 mm, coming from the double roller continuous casting process of CVG ALUCASA (Venezuela) was used. The chemical composition, obtained by optical emission spectroscopy, was (Wt. %): Mn 1.170, Fe 0.666, Si 0.357, Cu 0.133, Zn 0.012, Al 97.600.

Six samples were cut from the sheet. Three cuts, labeled as H samples, were subjected to a homogenization heat treatment in an electrical resistance oven, at 600 °C for 8 h as suggested by [7]., and then cooled slowly, while the other three, called DC samples, were left in its as-received condition. One of each H and DC samples were reserved for reference and labeled as initial condition (IC) samples (0 % cold work). One H sample and one DC sample were cold rolled with 30 % reduction in thickness, and the remaining samples were subjected to a 60 % reduction. The cold working process was carried out in an experimental rolling mill at a speed of 1.5 m/min, maintaining the original rolling direction of the sheet and making several passes. Afterwards, samples were cut for tensile testing specimen preparation and other cuts were made for microstructural evaluation.

The specimens for tensile tests were prepared as specified by the ASTM E8 [8]. standard with a rectangular cross section, 25 mm calibrated length and 100 mm total length. They were cut using the waterjet process to avoid microstructural changes in the cutting zone.

The samples for microstructural evaluation were finally embedded in polymethylmethacrylate to facilitate their handling and preparation, as well as to avoid possible contamination of the surface. Were prepared in accordance with the ASTM E3 [9]. and ASTM E407 [10]. standards, roughed down in water with sandpaper No. 240, 320, 400, 600 and 800. Afterwards, they were polished in two stages; first, with 1  $\mu$ m alumina, and then in a Buehler Electromet 4 electrolytic polishing machine with an electrolyte composed of 800 cm<sup>3</sup> of ethanol, 140 cm<sup>3</sup> of distilled water and 60 cm<sup>3</sup> of 60 % perchloric acid, applying a tension of 17 V for 25 seconds. Finally, samples were etched by immersion in a solution composed of 50 cm<sup>3</sup> of distilled water and 5 g of NaOH at 70 °C for 10 seconds.

#### 2.1.1. Optical microscopy (OM)

A preliminary exploration by optical microscopy is necessary in every microstructural characterization of materials, since it provides a general idea of the microstructure, distribution and morphology of the phases, and other features of interest in which to focus

with the electron microscopy techniques.

Samples were analyzed with an Olympus PMG3 microscope with magnifications from 100X to 1000X, and images were taken with an Olympus DP12 camera.

In this study, the expected variation of the microstructure due to deformation gradients was evaluated in three points cross section of the samples. These positions were termed «outer», «middle» and «center», as shown in Figura 1.

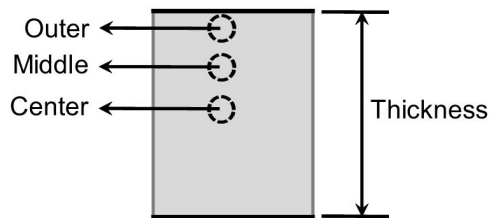


**Figure 1.** Positions to evaluate the variation of the microstructure cross section of the sample

### 2.1.2. Scanning electron microscopy (SEM)

This visualization technique was used to locate phases and precipitates in the microstructure to be identified later. This technique was selected because it is capable of greater image magnification (more than 1000X) compared with optical microscopy.

The sample surface was covered with gold dust, since this is a highly conductive material, enabling the electron scanning on the whole surface of the sample and obtaining images with improved resolution.

A JEOL JSM-6390 scanning electron microscope was used in the backscattered electron (BSE) configuration, a technique that highlights the contrast between phases, making them lighter or darker depending on the atomic weight of its components. In this method, the specific energy of the beam depends on the atomic number of the material, that is, the higher the average atomic number, the higher the intensity. The visualization was performed according to the pattern shown in Figure 1.

### 2.1.3. Energy dispersive X-ray spectroscopy (EDX) analysis

With this technique, it is possible to perform a semi quantitative chemical analysis of specific points or lines in the selected area of the sample. It gives values of the relative amount of the constituent elements expressed as weight percentage and as atomic weight, hence allowing the provisional identification of the observed phase. This analysis was performed with an Oxford Instruments 7582 EDX device.

### 2.1.4. Evaluation of the phases in the AA 3003 alloy

A tentative evaluation of the phases was performed with the results obtained from the SEM studies using a BSE detector, and the EDX analyzes, in conjunction with the investigations of [6, 7], [11, 12]. These authors have been able to identify, using TEM, two types of phases, both in the as-received and in the homogenized conditions:

- The primary phase, formed by the dendritic matrix of aluminum.
- The secondary phases  $Al_6(Mn,Fe)$  and  $\alpha-Al(Mn,Fe)Si$ , which may be part of the primary particles coming from the solidification of liquid with high content of alloying elements, and of the secondary particles (dispersoids, with size less than  $1 \mu m$ ), originating from the decomposition and precipitation of the alloying elements in supersaturated solid solution in the dendritic matrix.

### 2.1.5. Mechanical properties evaluation

Tensile tests were performed at a displacement rate of 5 mm/min using a 25-ton capacity MTS universal materials tester and a 1 in Instron extensometer. Five replications were carried out for each test condition, considering the longitudinal, transverse, and diagonal directions with respect to the rolling direction, evaluating a total of 90 specimens.

Vickers microhardness tests were performed on the samples used in optical microscopy, applying three penetrations for each study condition, according to the ASTM E384 [13]. standard. with a load of 50 g and 15 seconds of application. A Buehler Identamet 1104 Vickers - Knoop microhardness tester was used.

## 3. Results and discussion

### 3.1. Optical microscopy

This technique was used to identify points of interest, as well as the arrangement and preliminary morphology of the precipitates. For this reason, only results for the IC samples are presented. Figure 2 shows a scanning of the microstructure of the AA-3003 in the outer, middle, and center positions of the thickness, in the DC initial condition.

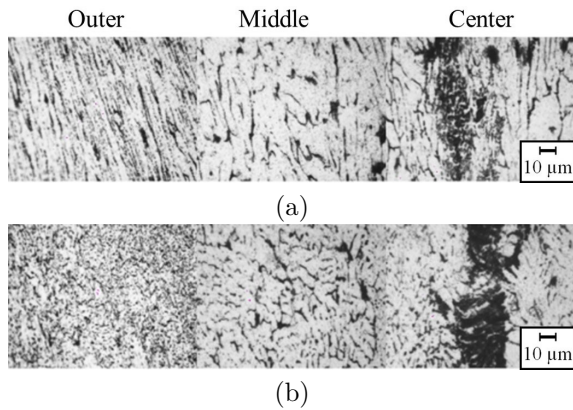


**Figure 2.** OM micrographs showing the microstructure of DC IC samples of AA 3003 alloy: (a) rolling direction, (b) transverse direction

It can be observed in Figure 2 (a) that the precipitates in the outer area are stretched in the direction of rolling. In contrast, in Figure 2(b) they show as dots, which is consistent with the stretching of the precipitates in the direction normal to the plane of the micrograph.

A characteristic of the DC continuous casting process is the temperature gradient across the thickness of the sheet, causing different cooling and solidification rates and producing a change of the microstructure, see Figures 2 (a) and (b). It can be observed that the precipitates are finer and are present in greater quantity at the outer areas of the samples, while in the middle zone the precipitates are larger and with lower density. A central segregation line (CSL) was observed towards the center area of the samples, which consists of a high concentration of precipitates aligned in the rolling direction. This defect, characteristic of aluminum alloys obtained by DC continuous casting, has been observed by other researchers [14, 15].

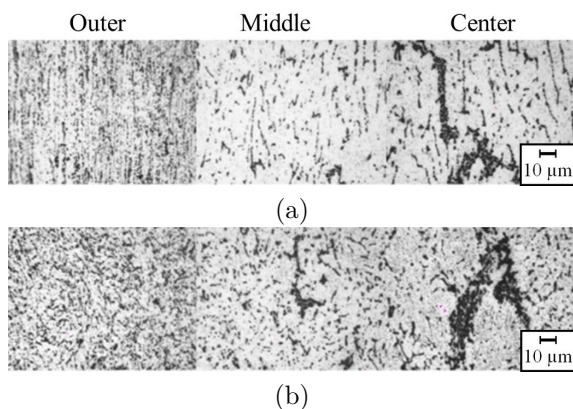


**Figure 3.** OM micrographs showing the microstructure of H IC samples of AA 3003 alloy: (a) rolling direction, (b) transverse direction

An expected result of the homogenization is the uniform distribution of the second phase particles, and

the absence of the CSL. However, although Figure 3 shows that the concentration of the precipitates in the CSL has been reduced, the distribution of the precipitates across the thickness is similar to that of the DC initial condition, see Figure 2. These facts lead to the conclusion that it is necessary to optimize the homogenization heat treatment parameters.

An additional effect of the homogenization is a change in the morphology of the precipitates. The micrograph of the as-received IC specimen in Figure 4 (a) shows the precipitates stretched in the direction of rolling, whereas Figure 4 (b) clearly shows the spheroidization of the precipitates in the homogenized IC specimen.

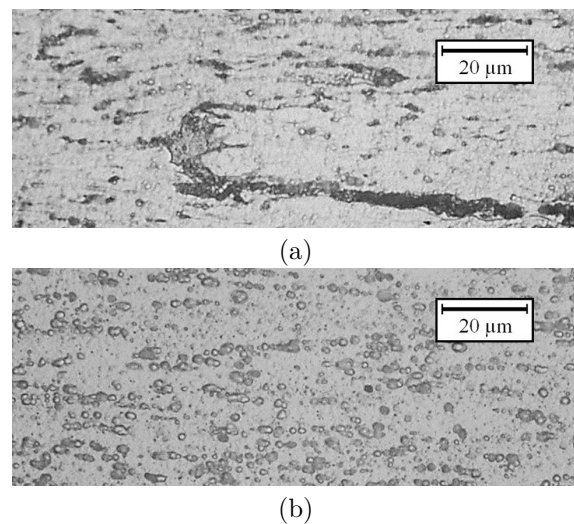


**Figure 4.** OM micrographs showing the effect of the homogenization in the morphology of the precipitates in the IC samples of AA 3003 alloy: (a) Stretched precipitates in the DC specimen, (b) spheroidized precipitates in the H specimen

### 3.2. Evaluation of phases by SEM

The evaluation of the phases of the IC specimens was performed using SEM with the BSE technique. The lighter regions in the images indicate the possible presence of the  $\alpha$ -Al(Mn,Fe)Si phase due to its high average atomic number (rich in Mn, Fe and Si), while the  $Al_6$ (Mn,Fe) phase has a smaller amount of Mn and Fe, thus a lower average atomic number and lower brightness than the  $\alpha$  phase. The matrix is the opaqueness phase, as it has the lowest concentration of the alloying elements.

Figure 5 and Table 1 show the microstructure of the alloy in the as received condition. According to [16], the constituent particles  $Al_6$ (Mn,Fe) and  $\alpha$ -Al(Mn,Fe)Si are formed mainly as interdendritic eutectic networks.

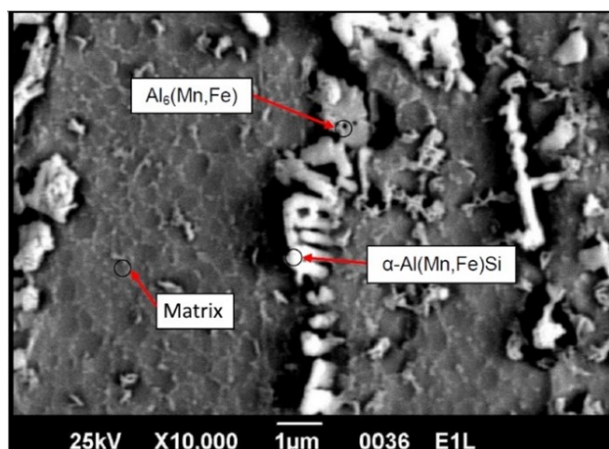


**Figure 5.** SEM micrograph showing the tentative identification of the phases of the AA-3003 alloy in the as received condition

**Table 1.** BSE chemical microanalysis of the AA-3003 alloy in the as-received condition

Phases	Weight percentage				Atomic percentage			
	Al	Mn	Fe	Si	Al	Mn	Fe	Si
Matrix	97	1,9	0,8	–	99	0,9	0,4	–
$\alpha$ -Al(Mn,Fe)Si	87	2,7	4,1	2	88	1,3	2	2
$Al_6$ (Mn,Fe)	89	3,1	5,3	–	90	1,5	2,6	–

It can be seen in Figure 5 that two phases coexist in eutectic networks, which are presumed to be those suggested by [16]. The semi quantitative chemical analysis and the analysis of EDX spectra performed at the points indicated in Figure 5 provide the following results:

- The evaluation in the area pointed as the matrix presents lower amounts of alloying elements compared to the other two, and absence of silicon.
- The phase marked as  $Al_6$ (Mn,Fe) has the highest iron content of the three zones evaluated, and there is no presence of silicon.
- The phase marked as  $\alpha$ -Al(Mn,Fe)Si is the only zone that has silicon.

These results show that the material in the DC condition has a microstructure that could be composed of  $Al_6$ (Mn,Fe) and  $\alpha$ -Al(Mn,Fe)Si.

Figure 6 and Table 2 show the microstructure of the homogenized material. The secondary phases appear as individual particles, in contrast to the eutectic networks shown in the material in the as-received condition. These particles, around 1  $\mu$ m in size, are classified as dispersoids.

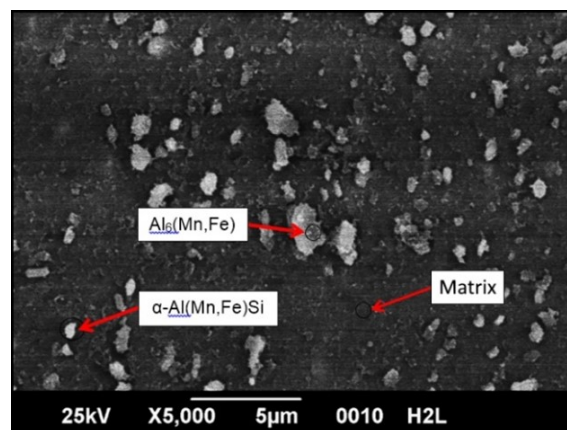


**Figure 6.** SEM micrograph showing the tentative identification of the phases of the AA-3003 alloy in the homogenized, 0 % cold work condition.

**Table 2.** BSE chemical microanalysis of the AA-3003 alloy in the homogenized, 0 % cold work condition

Phases	Weight percentage				Atomic percentage			
	Al	Mn	Fe	Si	Al	Mn	Fe	Si
Matrix	100	–	–	–	100	–	–	–
$\alpha$ -Al(Mn,Fe)Si	79,9	4,72	3,20	2,34	76,5	2,18	1,48	2,15
$Al_6$ (Mn,Fe)	86,3	3,47	3,94	–	84,2	1,66	1,88	–

Throughout the SEM evaluation of the homogenized material, it was difficult to locate particles whose chemical composition corresponded to the  $Al_6$ (Mn,Fe) phase. Therefore, it can be inferred that most of this phase transformed into the  $\alpha$ -Al(Mn,Fe)Si phase as a result of the heat treatment, as suggested by [6] and [11]. This effect increases the ductility of the alloy, improving its performance in plastic forming processes [6] [11].

The results obtained from the chemical analysis and the EDX spectra, presented in Figure 6, show that, as was the case with the as-received material, the dark phase contains the highest quantity of iron, and only the bright phase contains silicon. However, it can be noticed that the matrix is composed of 100 % aluminum, which evidences a decrease of the alloying elements in the supersaturated solid solution as a consequence of the applied heat treatment. Hence, the alloy reaches an equilibrium state through the precipitation of manganese and iron.

### 3.3. Structure and composition of the phases

During the heating to the homogenization temperature, the dispersoids precipitate in the matrix; afterwards, most of the primary particles composed of the  $Al_6$ (Mn,Fe) phase are transformed to the  $\alpha$ -Al(Mn,Fe)Si phase due to the high diffusion of the silicon contained in the solid and eutectics solutions [17–19]. Since transference of the silicon atoms does not

occur from one constituent to another (from primary particles to dispersoids or vice versa), neither interstitially nor by substitution, these researchers have proposed to study the evolution of primary and dispersoid particles through the ratio of the atomic percentages of Mn and Fe, obtained by the EDX spectra.

Li and Arnberg [16]. found that this ratio varies according to the temperature and time of homogenization, since the iron and manganese atoms mutually substitute in the primary and dispersoid particles. Based on this methodology, EDX and semiquantitative chemical analyzes were performed to primary and dispersoids particles located in the center and middle positions (see Figure 1) of both initial condition samples. Figures 7 and 8 show examples of the obtained EDX spectra, and Table 3 presents the elemental chemical composition and average Mn/Fe ratio.

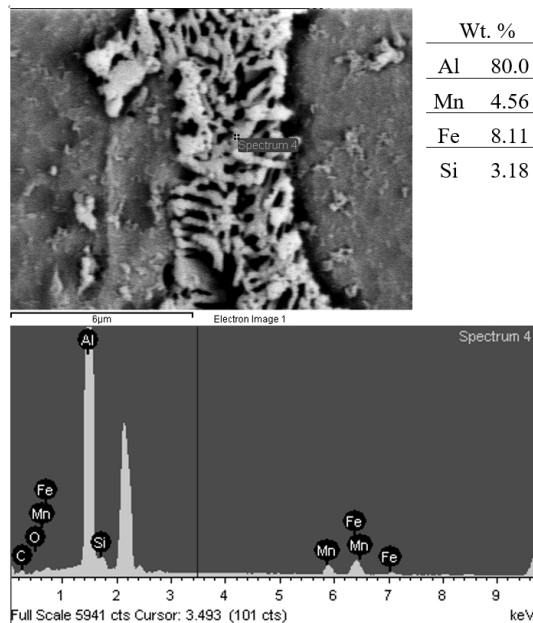


**Figure 7.** SEM micrograph and EDX spectrum of a primary particle in the as-received condition

**Table 3.** Elemental chemical composition obtained by EDX of the primary and dispersoid particles of the AA 3003 alloy in the DC and H initial conditions (Two samples per condition)

Particles	Initial condition	Weight percentage				Average Mn/Fe ratio
		Al	Mn	Fe	Si	
Primary	DC	80	4,6	8,1	3,2	0,57
		82	4,9	8,6	4,5	
	H	77	5,2	6,6	4,1	0,8
Dispersoids	H	77	6	4	3,1	1,56
		79	5,7	3,6	3,8	

Note: Two samples per condition

These results are similar to those found by [15], who obtained Mn/Fe ratios, for the primary particles,

of 0.57 in the DC condition, and 0.79 for the homogenized material; in the case of the dispersoids, a value of 1.70 was found.

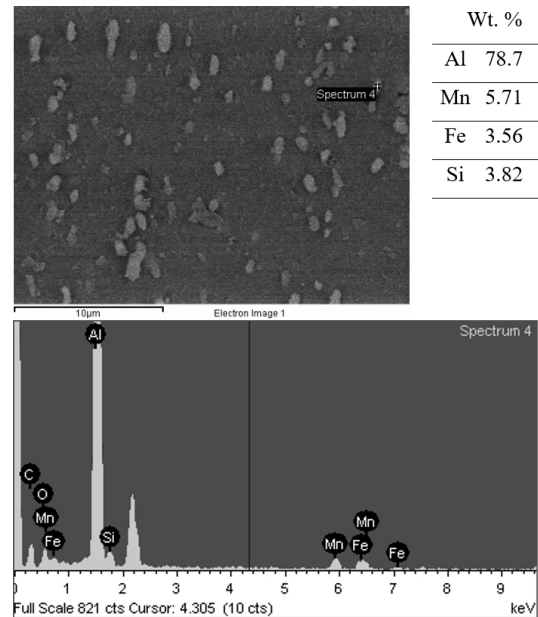


**Figure 8.** SEM micrograph and EDX spectrum of a dispersoid particle in the homogenized condition

Based on the similarity between our results and those found in the literature, it is presumed that there exist two types of  $\alpha$ -Al(Mn,Fe)Si phases in the homogenized condition:

- The primary  $\alpha$  phase, coming from the transformation of  $\text{Al}_6(\text{Mn,Fe})$  and from the rupture of eutectic networks during heating, which, similarly to the primary particles in the DC condition, have a high iron content.
- The secondary  $\alpha$  phase, coming from the precipitation and subsequent thickening of the dispersoids, differentiated from the primary  $\alpha$  phase due to its lower iron content, higher Mn/Fe ratio and smaller size. In this work, the few dispersoids that could be observed had a size that was always slightly larger than  $1 \mu\text{m}$  due to the thickening process during homogenization.

Since iron has very little solubility in solid aluminum, the decrease of the iron content in the primary particles for the homogenized material might indicate that not all the dispersoids in contact with the primary particles are dissolved and absorbed, but some of them may be exchanging manganese atoms for iron atoms with the primary particles. This could be the reason by which some dispersoids grew larger than  $1 \mu\text{m}$  in size and even became primary particles.

The compound tentatively identified as  $\alpha$ -Al(Mn,Fe)Si was the highest weight fraction phase

found in the alloy in the H condition, as was verified through the SEM evaluation as well as in the DC condition. This might be due to the high amount of silicon (0.357 % by weight) contained in the alloy employed in this work compared to those used by other authors (0.1 % to 0.2 % by weight), since a silicon content exceeding a weight percentage of 0.07 favors the precipitation of the  $\alpha$  phase; in contrast, a lower silicon content will promote the precipitation of the  $\text{Al}_6(\text{Mn,Fe})$  phase [17].

Another finding in some areas of the samples in the DC condition was the presence of rectangular shaped precipitates identified, with the help of EDX analyses, as  $\text{Al}_6\text{-}_7\text{Mn}$ , see Figure 9. Similar precipitates, in shape and composition, were observed by [15] and [19], in samples of sheets of AA 3003 obtained by continuous casting. Therefore, this might be a characteristic precipitate morphology of this material.

Moreover, note in Figure 9 that the length of these precipitates is less than  $1\ \mu\text{m}$ ; therefore, they can be classified as dispersoids. These particles precipitate in the dendritic zones during the continuous casting process at approximately  $350\ \text{°C}$ , temperature at which the precipitation of dispersoids initiates.

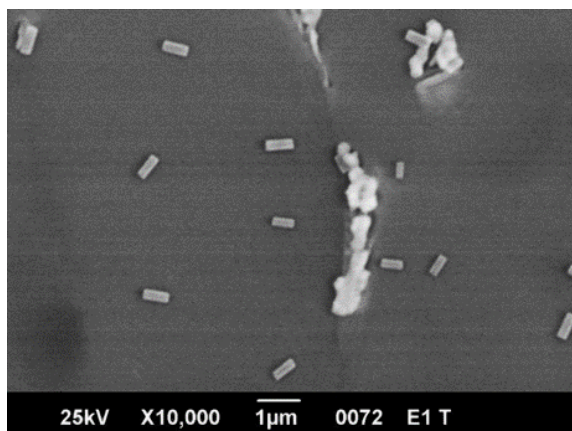


**Figure 9.** SEM micrograph showing  $\text{Al}_6\text{-}_7\text{Mn}$  precipitates in DC samples

### 3.4. Variation of the microstructure with cold working

The sheets of aluminum alloys obtained by continuous casting exhibit a higher concentration of alloying elements in supersaturated solid solution, and smaller intermetallic (eutectic) particles, as compared to other types of casting. These characteristics affect the thermo-mechanical behavior of the alloy during the forming processes. SEM micrographs of the DC and H samples, subjected to cold working as described in the Experimental section, were acquired to investigate this phenomenon and to determine the influence of both the cold working and the homogenization heat treatment on the distribution of the phases. Figure 10 shows the SEM micrographs for the DC material, with and without cold working, of the outer and center positions of the samples.

It can be observed in Figure 10 (a) the formation of eutectic networks in its initial stage, and columnar dendritic structures, both elongated in the direction of lamination, in the outer zone of the sample. This is caused by the direct contact of the surface of the sheet with the roller during the casting process; therefore, it is the zone subjected to the highest cooling rate and pressure.

The variation of the microstructure distribution with the amount of cold work applied is shown in Figure 10 (b) and (c). As the cold deformation increases, so does the separation of the primary and secondary particles contained in the interdendritic and dendritic regions, respectively. Furthermore, the number of primary particles is also increased, but their size is reduced.

Figure 11 shows an image of the central zone in a DC sample, where a CSL can be noticed. This line was observed in all samples of the DC material, which confirms an appropriate control of the process and a good efficiency in the extraction of the heat by both rollers. It was found in an EDX line profile analysis performed to the CSL that as the central zone is approached, there is a reduction of the aluminum concentration and an increase of the alloying elements, mainly iron, due to its low solubility in solid aluminum.

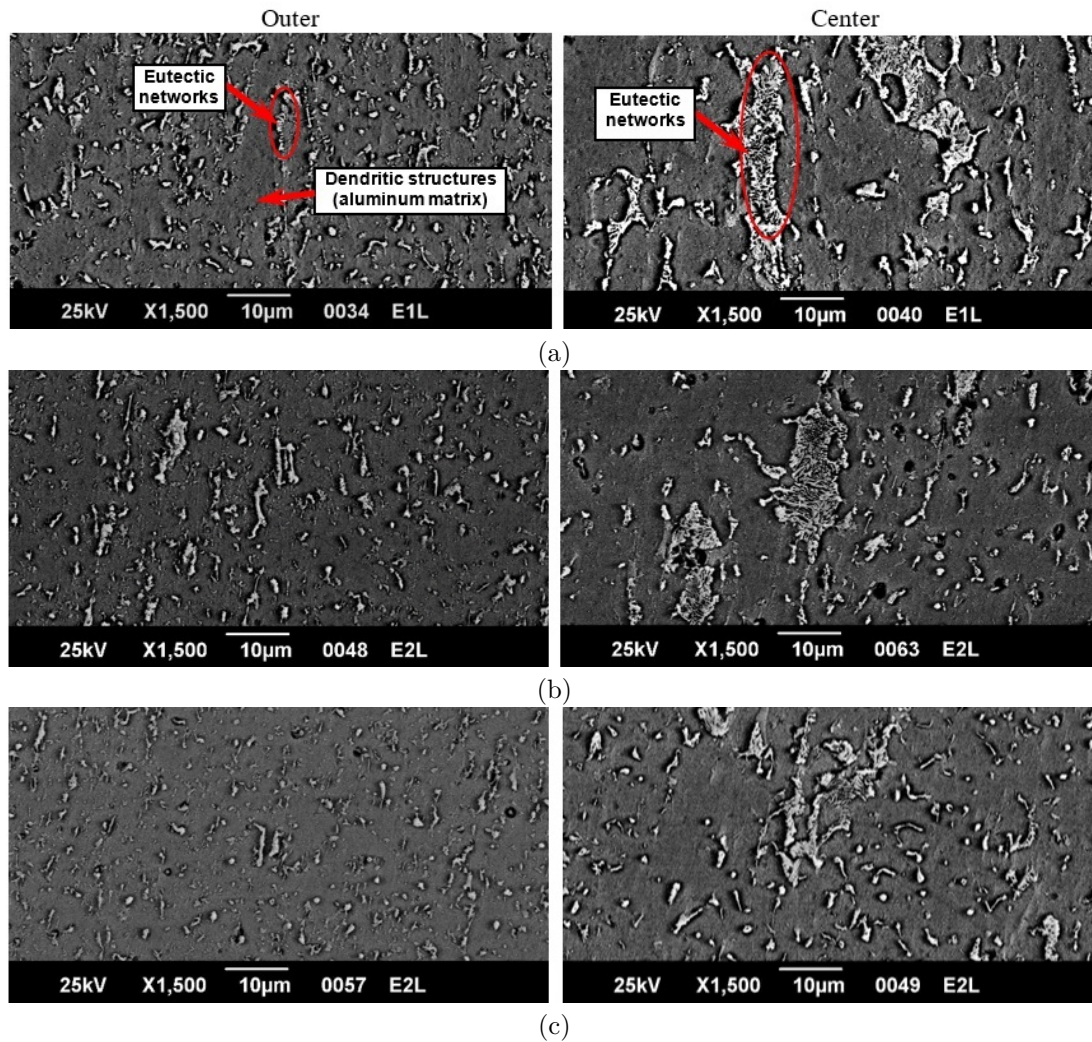


**Figure 10.** SEM micrographs showing the variation of the microstructure of the AA-3003 as-received sample with cold working, at the outer and center positions: (a) 0 % CW, (b) 30 % CW, and (c) 60 % CW

Figure 12 shows the CSL after homogenization, confirming the decrease in the number of segregates, as compared to Figure 11.

Figure 13 shows the SEM micrographs for the homogenized material, with and without cold working, of the outer and center zones of the samples. In this case, particles with an average size of 2 to 3  $\mu\text{m}$  were observed at the outer position of the sample, while in the center they have a larger size, from 3 to 5  $\mu\text{m}$ . This occurs because the formers originate from the rupture of eutectic networks which are much smaller than those observed in the middle and center positions.

In Figure 13 (a), the particles are grouped in the form of what previously were the eutectic networks located in the interdendritic regions. As the level of cold working increases, these particles are displaced by the effect of the movement of the sliding planes, leading to the loss of these clusters and showing further alignment of the precipitates with the direction of lamination (See Figures 12, 13 (a) and 13 (b)).

Note in Figure 13 that, in contrast to the variation of the microstructure for the DC condition, no substantial change in the size of the secondary phase particles was observed with the increase of the cold working in the homogenized samples. This condition contributes to the homogeneity of the mechanical properties, which is an evidence of the effectiveness of the application of the homogenization heat treatment prior to a cold forming process.

Torres *et al.* [20]. determined that a higher diffusion rate, which increases with the time of homogenization, induces a greater localized dissolution of the CSL and, at the same time, a redistribution of the segregates in the aluminum matrix, producing a more uniform microstructure.

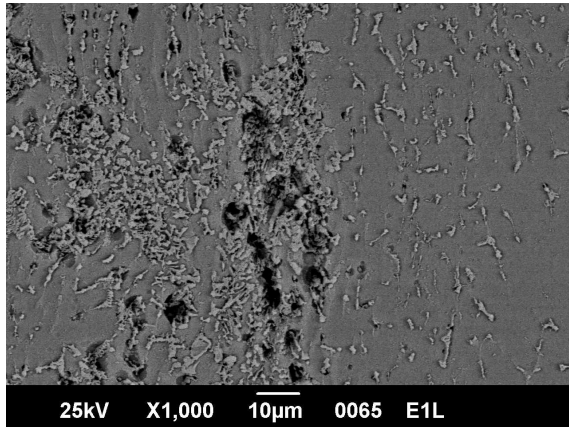


Figure 11. SEM micrographs showing the CSL for the as-received material

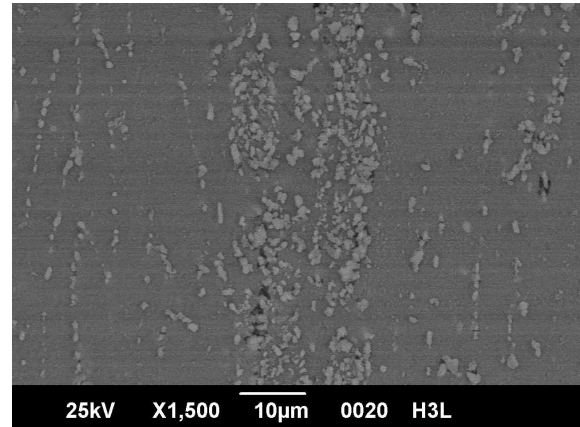


Figure 12. SEM micrographs showing the CSL for the homogenized material

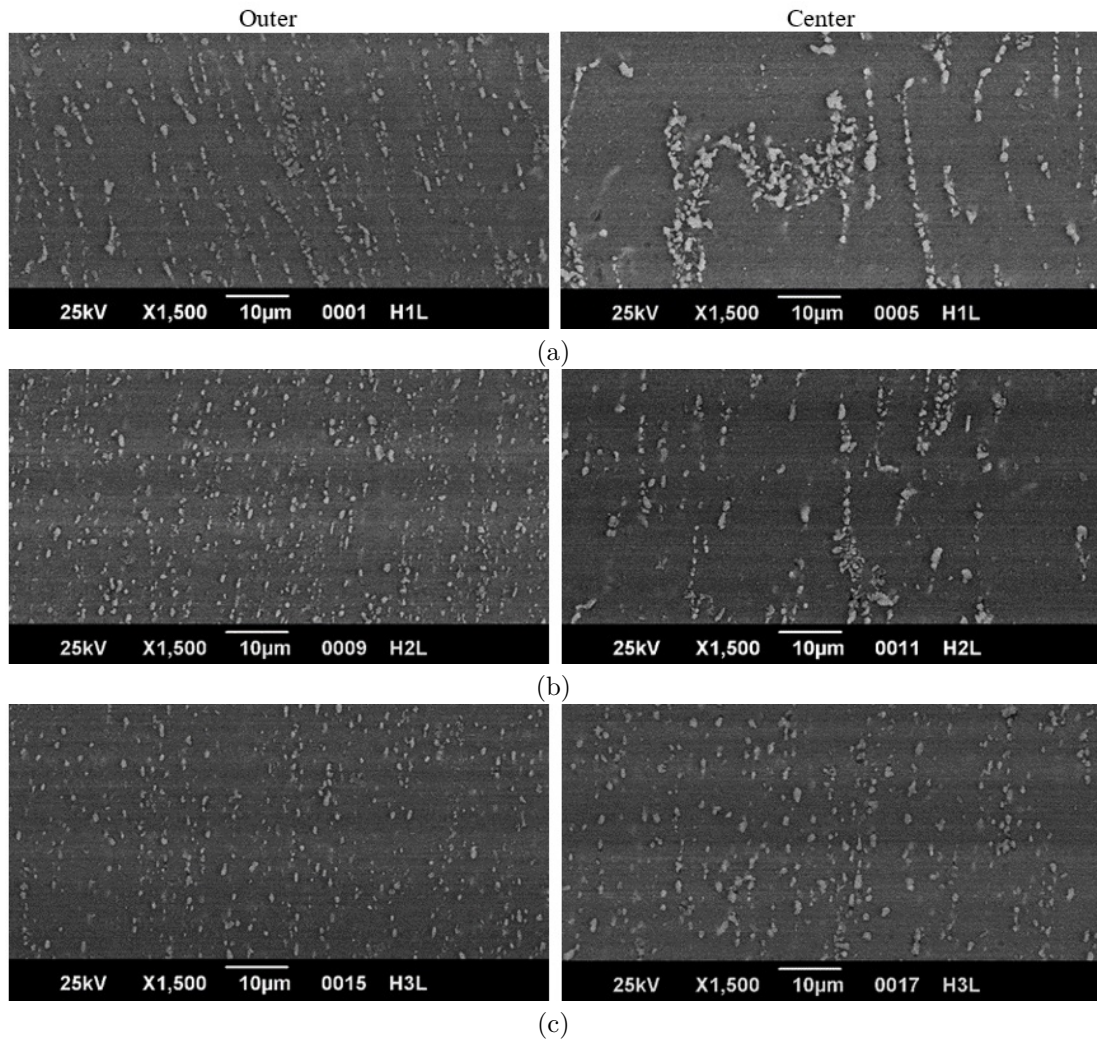


Figure 13. SEM micrographs showing the variation of the microstructure of the AA-3003 homogenized sample with cold working, at the outer and center positions: (a) 0 % CW, (b) 30 % CW, and (c) 60 % CW

### 3.5. Mechanical properties

Table 4 shows the mean and standard deviation of the mechanical properties obtained from the tensile and microhardness tests. Yield strength ( $S_{0,2}$ ), tensile strength ( $S_u$ ), ductility as a function of percent reduction in area (RA) and Vickers microhardness (HV) are reported.

**Table 4.** Mechanical properties of AA3003 in the DC and H conditions as a function of cold work

Initial Cond.	Properties	Cold Work (%), mean (SD)		
		0	30	60
DC	$S_{0,2}$ (MPa)	102 (1,99)	200 (3,10)	243 (4,30)
	$S_u$ (MPa)	161 (0,054)	209 (0,920)	251 (1,50)
	RA (%)	53,9 (1,64)	43,1 (2,56)	28,6 (4,32)
	HV	52,8 (4,65)	70,8 (4,30)	78,4 (3,92)
H	$S_{0,2}$ (MPa)	44,5 (2,17)	148 (1,01)	187 (2,40)
	$S_u$ (MPa)	112 (0,360)	155 (1,14)	195 (1,74)
	RA (%)	64,1 (2,59)	59,9 (0,480)	46,3 (5,63)
	HV	38,3 (2,03)	51,7 (4,96)	62,1 (2,75)

Table 4 shows the increase in strength and hardness, and the decrease in ductility, as the cold work is increased regardless of the initial condition of the material, which is due to the strain hardening mechanism of this alloy and is related to the generation, movement and stacking of dislocations at the grain boundaries or different obstacles that the crystal may present.

The differences in strength and hardness between the as-received and homogenized materials are mainly due to two mechanisms: the first and dominant one is the constraining of the movement of dislocations by the presence of more alloying element atoms in supersaturated solid solution in the DC condition, which was confirmed by the EDS spectrum shown in Figure 7; the second mechanism is the hardening by the dispersion of small particles in the matrix, such as the Al<sub>6</sub>-7Mn precipitates found in the DC condition and shown in Figure 9 which, according to some researchers, are incoherent with the matrix and promote the formation of dislocation rings around them, thus further hardening the aluminum matrix [19], [21].

Table 5 shows the percentage difference of the mechanical properties relative to the maximum amount of cold work, which was 60%. Comparing these results, for the homogenized material prior to cold working (H) a much higher increase in strength (320 % compared to 138 % for the DC material) and hardness (62.1 % compared to 48.5 % for the DC material), and a smaller decrease in ductility (-27.8 % compared to -46.9 % for the DC material) were obtained.

These results indicate that homogenization prior to cold working considerably improves the cold plastic deformation capacity of the alloy, since the decrease in ductility measured as a function of area reduction is

much lower than that obtained without prior homogenization. On the other hand, although the homogenized material does not reach the strength and hardness of the direct cast alloy, by making a comparison for the same deformation percentages, the increases in these properties are more significant, which indicates that by continuing the cold plastic deformation process, a material with higher strength and hardness would be obtained, in addition to the higher cold deformation capacity.

These results correlate with those obtained in section 3.4, showing that the homogenization process of the AA3003 alloy from continuous casting improves its plastic deformation capacity and decreases the probability of cracking during subsequent cold working.

**Table 5.** Percentage differences of the mechanical properties of AA3003 for the DC and H conditions with respect to the maximum amount of cold work (60 % CW).

Properties	Percentage difference	
	DC	H
$S_{0,2}$ (MPa)	138	320
$S_u$ (MPa)	55,9	74,1
RA (%)	-46,9	-27,8
HV	48,5	62,1

## 4. Conclusions

Based on the results obtained for the different evaluated conditions, the secondary phases were tentatively identified as Al<sub>6</sub>(Mn,Fe) and  $\alpha$ -Al(Mn,Fe)Si, which varied in quantity, size, and shape. A conclusive identification requires a TEM analysis, which was not possible at the time of this investigation.

Secondary phases are composed of primary and secondary particles, which differ in their Fe and Mn content, resulting in a lower Mn/Fe ratio for the primary particles (0.57 for the as received condition and 0.80 for the homogenized condition), whereas the dispersoids have a higher Mn/Fe ratio (1.56 after the homogenization).

The homogenization should be adjusted to a longer exposure time, since the secondary phase particles, aligned with the lamination direction, could still be observed in the microstructure.

The homogenization produces the decomposition of the supersaturated solid matrix through the dissolution and precipitation of dispersoids, in addition to spheroidizing the primary particles contained in the interdendritic zones. Because of these effects, the ductility of the material is expected to increase, thus producing favorable conditions for the application of cold forming processes. The application of the cold

working to the unhomogenized material caused the division and separation of the particles of the secondary phases. In contrast to this behavior, the particles of the previously homogenized material showed minor variation of their size. This is a desirable condition for subsequent metal forming applications because of the lower probability of cracking of the material during cold working.

The above was confirmed by the results obtained for strength, hardness, and ductility, which showed an increase of 320 % in yield strength and a decrease in ductility of 27.8 % for the homogenized material, compared to 138 % and 46.9 %, respectively, for the untreated material, thus demonstrating that the homogenized material has a greater capacity for cold plastic deformation.

## Acknowledgements

To the CDCH of Universidad de Carabobo for funding this research.

To the Scanning Electron Microscopy and Optical Microscopy laboratories of Universidad Simón Bolívar, and Materials Laboratory of Universidad de Carabobo, for allowing the use of the equipment used in this work.

## References

- [1] G. Aparicio, "Evaluación del comportamiento mecánico de la aleación de aluminio 3003 proveniente de colada continua," Master's thesis, 2010.
- [2] M. Dehmas, E. Aeby-Gautier, P. Archambault, and M. Serrière, "Interaction between eutectic intermetallic particles and dispersoids in the 3003 aluminum alloy during homogenization treatments," *Metallurgical and Materials Transactions A*, vol. 44, no. 2, pp. 1059–1073, Feb. 2013. [Online]. Available: <https://doi.org/10.1007/s11661-012-1473-1>
- [3] Y. J. Li and L. Arnberg, "Quantitative study on the precipitation behavior of dispersoids in DC-cast AA3003 alloy during heating and homogenization," *Acta Materialia*, vol. 51, no. 12, pp. 3415–3428, 2003. [Online]. Available: [https://doi.org/10.1016/S1359-6454\(03\)00160-5](https://doi.org/10.1016/S1359-6454(03)00160-5)
- [4] Y. Li and L. Arnberg, *Precipitation of Dispersoids in DC-Cast AA3103 Alloy during Heat Treatment*. Grandfield J.F., Eskin D.G. (eds) Essential Readings in Light Metals. Springer, Cham, 2016. [Online]. Available: [https://doi.org/10.1007/978-3-319-48228-6\\_129](https://doi.org/10.1007/978-3-319-48228-6_129)
- [5] M. Velandia and B. Hidalgo, "Evolución estructural de la aleación AA-3003 sometida a tratamiento térmico de homogenización," in *7th Latin American and Caribbean Conference for Engineering and Technology, San Cristóbal, Venezuela*, 2009. [Online]. Available: <https://bit.ly/3fofH1V>
- [6] H.-W. Huang and B.-L. Ou, "Evolution of precipitation during different homogenization treatments in a 3003 aluminum alloy," *Materials & Design*, vol. 30, no. 7, pp. 2685–2692, 2009. [Online]. Available: <https://doi.org/10.1016/j.matdes.2008.10.012>
- [7] Y. J. Li and L. Arnberg, "Precipitation of dispersoids in DC-cast 3003 alloy," in *Aluminium Alloys 2002 - ICAA8*, ser. Materials Science Forum, vol. 396. Trans Tech Publications Ltd, 7 2002, pp. 875–880. [Online]. Available: <https://doi.org/10.4028/www.scientific.net/MSF.396-402.875>
- [8] ASTM, *ASTM E8 / E8M-21, Standard Test Methods for Tension Testing of Metallic Materials*. ASTM International, West Conshohocken, 2004. [Online]. Available: [http://doi.org/10.1520/E0008\\_E0008M-21](http://doi.org/10.1520/E0008_E0008M-21)
- [9] —, *ASTM E3-01, Standard Practice for Preparation of Metallographic Specimens*. ASTM International, West Conshohocken, 2001. [Online]. Available: <http://doi.org/10.1520/E0003-01>
- [10] —, *ASTM E407-07(2015)e1, Standard Practice for Microetching Metals and Alloys*. ASTM International, West Conshohocken, 1999. [Online]. Available: <http://doi.org/10.1520/E0407-07R15E01>
- [11] M. Dehmas, P. Weisbecker, G. Geandier, P. Archambault, and E. Aeby-Gautier, "Experimental study of phase transformations in 3003 aluminium alloys during heating by in situ high energy X-ray synchrotron radiation," *Journal of Alloys and Compounds*, vol. 400, no. 1, pp. 116–124, 2005. [Online]. Available: <https://doi.org/10.1016/j.jallcom.2005.03.062>
- [12] G. E. Totten and D. S. MacKenzie, *Handbook of Aluminum: Vol. 1: Physical Metallurgy and Processes*. CRC Press, 2003. [Online]. Available: <https://bit.ly/2SqMkTE>
- [13] ASTM, *ASTM E384-17, Standard Test Method for Microindentation Hardness of Materials*, ASTM International, West Conshohocken ed., 2002. [Online]. Available: <http://doi.org/10.1520/E0384-17>
- [14] J. Pérez-Illzarbe Uriz, J. Faustmann Salas, and A. Suárez Sanabria, "Recristalización de bandas de aluminio procedentes de colada continua, laminadas en frío," *Revista de Metalurgia*, vol. 36, no. 6, pp. 435–451, 2000. [Online]. Available: <https://dx.doi.org/10.3989/revmetalm.2000.v36.i6.594>

- [15] M. Slámová, M. Karlík, F. Robaut, P. Sláma, and M. Véron, “Differences in microstructure and texture of Al-Mg sheets produced by twin-roll continuous casting and by direct-chill casting,” *Materials Characterization*, vol. 49, no. 3, pp. 231–240, 2002. [Online]. Available: [https://doi.org/10.1016/S1044-5803\(03\)00011-1](https://doi.org/10.1016/S1044-5803(03)00011-1)
- [16] Y. J. Li and L. Arnberg, “Evolution of eutectic intermetallic particles in DC-cast AA3003 alloy during heating and homogenization,” *Materials Science and Engineering: A*, vol. 347, no. 1, pp. 130–135, 2003. [Online]. Available: [https://doi.org/10.1016/S0921-5093\(02\)00555-5](https://doi.org/10.1016/S0921-5093(02)00555-5)
- [17] M. Poková, M. Cieslar, and J. Lacaze, “Enhanced aw3003 aluminum alloys for heat exchangers,” in *WDS’11 Proceedings of Contributed Papers, Part II*, 2011, pp. 141–146. [Online]. Available: <https://bit.ly/3bYehcj>
- [18] M. M. R. Jaradeh and T. Carlberg, “Solidification studies of 3003 aluminium alloys with Cu and Zr additions,” *Journal of Materials Science & Technology*, vol. 27, no. 7, pp. 615–627, 2011. [Online]. Available: [https://doi.org/10.1016/S1005-0302\(11\)60116-3](https://doi.org/10.1016/S1005-0302(11)60116-3)
- [19] J. P. Martins, A. L. M. Carvalho, and A. F. Padilha, “Microstructure and texture assessment of Al-Mn-Fe-Si (3003) aluminum alloy produced by continuous and semicontinuous casting processes,” *Journal of Materials Science*, vol. 44, no. 11, pp. 2966–2976, Jun. 2009. [Online]. Available: <https://doi.org/10.1007/s10853-009-3393-z>
- [20] T. Torres, R. Bisbala, S. Cameroa, and C. Llanos, “Estudio del efecto del tratamiento térmico de homogeneización en la microestructura y propiedades mecánicas de una aleación de aluminio AA8011,” *Acta Microscópica*, vol. 20, no. 2, pp. 165–173, 2011. [Online]. Available: <https://bit.ly/3wCbT2K>
- [21] S. Y. Paredes-Dugarte and B. Hidalgo-Prada, “Micromecanismo de deformación durante la laminación en frío de la aleación comercial de aluminio 3003,” *Suplemento de la Revista Latinoamericana de Metalurgia y Materiales*, no. 2, pp. 778–781, 2009. [Online]. Available: <https://bit.ly/2SpEYQh>